Scholars Journal of Engineering and Technology
OPEN ACCESS
Abbreviated Key Title: Sch J Eng Tech
ISSN 2347-9523 (Print) | ISSN 2321-435X (Online)
Journal homepage: https://saspublishers.com

A Density Functional Theory Investigation of the Fragmentation Mechanism of Deprotonated β-alanine

Quan Sun[1*], Hongjie Qu[1], Qiang Li[1], Dongxue Ding[1], Lili Cao[1], Juan Chen[1], Bo Wang[1]

[1]College of Science, Heilongjiang Bayi Agricultural University, Daqing, 163319, Heilongjiang Province, P. R. China

DOI: 10.36347/sjet.2022.v10i07.006 | **Received:** 17.06.2022 | **Accepted:** 21.07.2022 | **Published:** 22.07.2022

***Corresponding author:** Quan Sun
College of Science, Heilongjiang Bayi Agricultural University, Daqing, 163319, Heilongjiang Province, P. R. China

Abstract **Review Article**

In this paper, density functional theory (DFT) was applied to study the isomerization process and fragmentation mechanism of deprotonated β-alanine ions ([β-Ala–H]$^-$) at B3LYP/6-311++G(2df,2pd) level. The potential energy profiles of the [β-Ala–H]$^-$ in isomerization, H_2O- and NH_3-loss reaction pathways were plotted using relative to analyze preferred dissociation pathways and the structure of the resulting molecular ion products. In addition, the effect of temperature on reaction pathways and dissociative products were also investigated. The results show that **a2** structure is the most stable configuration of [β-Ala–H]$^-$, and the reaction barrier required for hydrogen transfer (47.76 ~ 54.02 kcal·mol^{-1}) is higher during isomerization. **Path 10** ($\Delta G^{\neq}$ = 50.77 kcal·mol^{-1}) is the dominant pathway of all the NH_3-loss reaction, and the corresponding product **p3** is also the dominant product in the deamination products. **Path 1** is the dominant pathway in H_2O-loss reaction. Meanwhile, temperature has no effect on dehydration and deamination reaction mechanism.

Keywords: deprotonated β-alanine ions, reaction mechanism, H_2O-loss pathways, NH_3-loss pathways.

1. INTRODUCTION

β-alanine is the simplest β-amino acid which plays an important role in a variety of biological processes. It is found in the brain and liver tissues of animals, as well as in the cuticle of plants, fruits and insects [1]. β-alanine is also a non-essential amino acid [2, 3] which is present in low concentrations in neural tissue [4, 5] and visual system [6]. There are two industrial methods for preparing β-alanine: the one is acrylonitrile-amino-acetic acid synthesis [7], and the other is fatty acid tricarboxylic acid cycle synthesis [8]. Since 2008, β-alanine has been widely used as a supplement in energy drinks [2, 9-11]. In addition, β-alanine also have great significance in molecular design [12, 13], drug synthesis [14-17], medical detection [18] and interstellar exploration [19, 20].

The crystal of β-alanine is orthorhombic with the space group Pbca, the unit cell of dimensions is a = 9.822, b = 13.807, c = 6.086 Å [21, 22]. β-alanine exists as zwitter-ion form in both crystal [23, 24] and aqueous solutions [25]. In 1995, McGlone studied the rotational spectra of the gas phase structure of β-alanine by experimental and theoretical calculations [26]. For some time afterwards, beta-alanine fell out of the spotlight. Until 2006, Sanz made β-alanine suitable for gas phase structure studies by combining Fourier transform microwave spectroscopy in pulsed supersonic jets with laser ablation, and they also discovered the first conformation stabilized by N–π* hyperconjugation between the amino nucleophile N: and the π* orbital on the carbonyl group [27].

Eckersley [28] obtained [Ala–H–H_2O]$^-$ and [Ala–H–NH_3]$^-$ proton-alanine fragments by fast atomic bombardment mass spectrometry (FAB-MS/MS), which Choi [29] did not obtain corresponding fragments by atmospheric pressure chemical ionization mass spectrometry (APCI-MS). Two of them only performed mass dissociation of α-amino acids, and the fragmentation mechanism is unknown.

The geometric configurations of the reactants, intermediates, transition states, product ions and neutral molecules of deprotic [β-Ala–H]$^-$ were optimized, the thermodynamic data were obtained by frequency analysis. The potential energy profiles of isomerization, H_2O- and NH_3-loss pathways of [β-Ala–H]$^-$ were constructed respectively, and then judge the dominant pathway and the dominant product. In addition, the influence of temperature on H_2O- and NH_3-loss

pathways, and dominant product were also analyzed in this study. The results will provide some model support for clarifying the fragmentation mechanism of deprotonated amino acid ions.

2. COMPUTATIONAL DETAILS

Imparity with β-alanine, β-alanineis not chiral. Therefore, [β-Ala–H]$^-$ is constructed directly as the investigated target in this study. The geometric configurations of all reactants, intermediates, transition states, products and dissociated neutral molecules were obtained by using B3LYP method [30-32] combined with 6-311++G(2df,2pd) base set [33] in corporated in the Gaussian09 program system [34]. After geometric optimization, frequency vibration calculation is carried out to determine the geometrical position is the minimum value (no virtual frequency) or transition state (only one virtual frequency). In addition, we also calculate the thermal correction of the key stability points at the same level in geometric optimization, and obtain their relative enthalpy of reaction and Gibbs free energy of relative reaction with temperature [35].

3. RESULT AND DISCUSSION

3.1 Isomerization of [β-Ala–H]$^-$

In this study, 33 isomers of [β-Ala–H]$^-$ were calculated, which could be divided into 5 groups according to the position of negative charge, whether the molecule formed a ring, and the *cis-trans* isomerism of the ring formed molecule. All the isomers of [β-Ala–H]$^-$ are shown in Figure 1. The and relative Gibbs-free energies (R.G., kcal·mol^{-1}) are all took **a2**, the lowest energy isomer, as reference point.

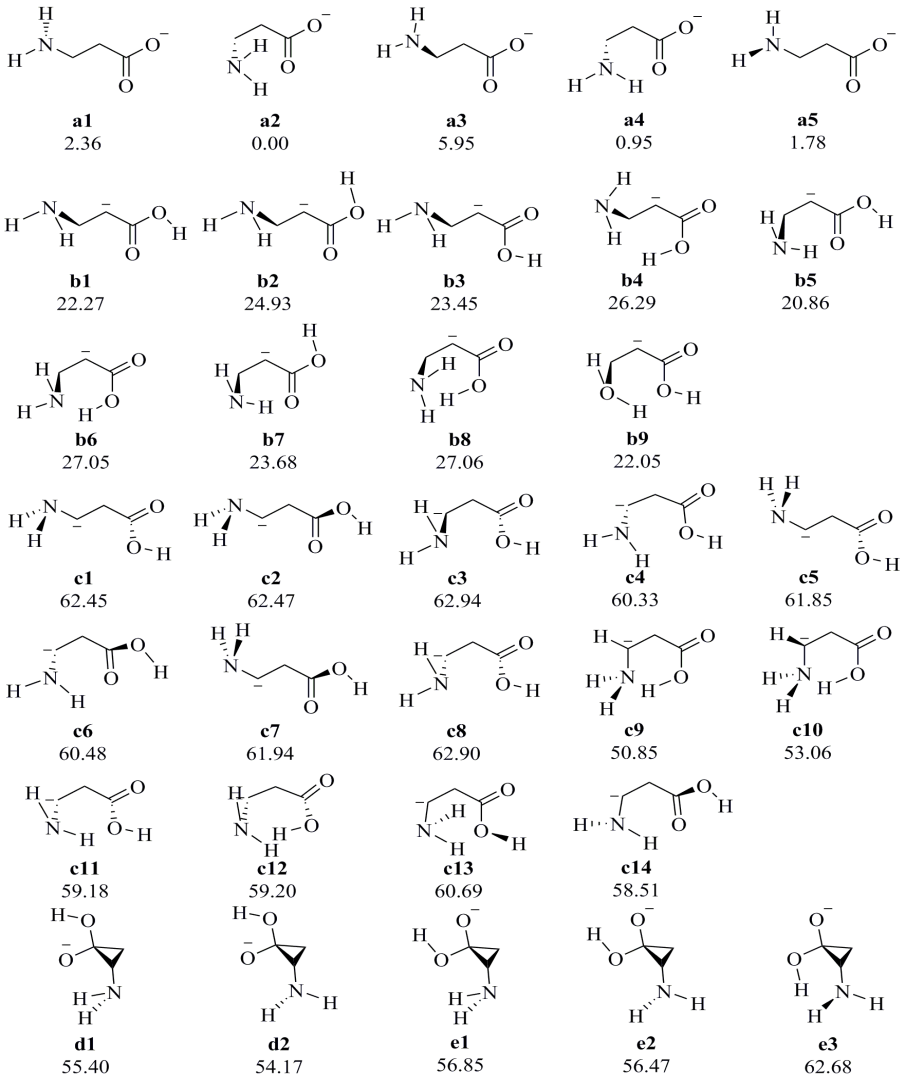

Figure 1: Thirty-three isomers of [β-Ala–H]$^-$ computed at the B3LYP/6-311++G(2df,2pd) level of theory with the temperature of 473.15 K

Among them, species **a** has the lowest energy whose negative charge is located on CO_2 (0.00 ~ 5.95 kcal·mol^{-1}); species **b** has a relatively high energy and the negative charge at α-C (20.86 ~ 27.06 kcal·mol^{-1}); and the energies of **c**, **d** and **e** anions are the highest, and the energies of these three anions are similar to each other (50.85 ~ 62.94 kcal·mol^{-1}). The energy drops dramatically from **c** to **a**. It can be seen from Figure 1, the negative charge of species **a** is in the carboxyl group, the negative charge of species **b** is on α-C, the

negative charge of species **c** is on β-C, and the negative charge of species **d** and **e** is on oxygen atom. Thus, from species **a** to **c**, the energy of [β-Ala–H]$^-$ ions increases and becomes unstable as the charge is transferred from the carboxyl group to β-C. From species **c** to **d** or β-C, although the charge is transferred back to the oxygen atom from β-C, the ion changes from chain structure to term-ring, which is greatly affected by Baeyer tension. Therefore, when the two factors reach equilibrium, the energy of species **d** and **e** structures is similar to that of species **c**.

Table 1 shows the isomerization process among 33 isomers of [β-Ala–H]$^-$. IsomerA and IsomerB represent the two ions before and after isomerization, TS represents the transition state, R.G. represents the relative Gibbs-free energies of the isomers and the transition states corresponding to **a2** as a reference point, C_α–C_β represents the σ bond rotation between α-C and β-C, NH_2-rot represents the amidogen rotation, C_{car}–OH represents the σ bond rotation between a carboxyl carbon atom and its bonded hydroxyl oxygen atom, C_{car}–C_α represents the σ bond rotation between a carboxyl carbon atom and a α-C atom, *H-vibration* means the vibration of a hydrogen atom, *cyclization* means the cyclic formation of species **c** into species **d** or **e**, *H-shift* represents the process of hydrogen transferation, and the relative barrier given by $\Delta G^{\neq}$ is the difference between the energy of the transition state and the average energy of the two isomers connected to the transition state. All energy units are kcal·mol^{-1}.

Table 1: Isomerization of 33 isomers of proton [β-Ala–H]$^-$

Isomer A	R.G.	TS	R.E.	Isomer B	R.G.	Isomerization	$\Delta G^{\neq}$	Isomer A	R.G.	TS	R.E.	Isomer B	R.G.	Isomerization	$\Delta G^{\neq}$
a1	2.36	**TS1**	7.77	**a3**	5.95	C_α–C_β	3.61	**c4**	60.33	**TS25**	66.05	**c6**	60.48	C_{car}–C_α	5.64
a4	0.95	**TS2**	5.95	**a1**	2.36	C_α–C_β	4.30	**c11**	59.18	**TS26**	65.43	**c4**	60.33	NH_2-rot	5.67
a5	1.78	**TS3**	4.01	**a1**	2.36	NH2-rot	1.94	**c5**	61.85	**TS27**	66.76	**c7**	61.94	C_{car}–C_α	4.87
a2	0.00	**TS4**	3.27	**a4**	0.95	NH2-rot	2.80	**c11**	59.18	**TS28**	65.31	**c5**	61.85	C_α–C_β	4.80
a2	0.00	**TS5**	5.23	**a5**	1.78	C_α–C_β	4.34	**c6**	60.48	**TS29**	69.29	**c8**	62.90	C_α–C_β	7.59
b6	27.05	**TS6**	33.14	**b8**	27.06	C_α–C_β	6.08	**c14**	58.51	**TS30**	65.07	**c6**	60.48	NH_2-rot	5.58
b1	22.27	**TS7**	29.24	**b2**	24.93	C_{car}–OH	5.64	**c14**	58.51	**TS31**	66.31	**c11**	59.18	C_{car}–C_α	7.47
b7	23.68	**TS8**	25.82	**b2**	24.93	NH2-rot	1.51	**c14**	58.51	**TS32**	65.53	**c7**	61.94	C_α–C_β	5.30
b5	20.86	**TS9**	23.21	**b1**	22.27	NH2-rot	1.64	**c14**	58.51	**TS33**	68.19	**c13**	60.69	C_α–C_β	8.59
b2	24.93	**TS10**	49.06	**b8**	27.06	C_{car}–C_α	23.06	**c13**	60.69	**TS34**	67.33	**c8**	62.90	NH_2-rot	5.53
b3	23.45	**TS11**	30.88	**b8**	27.06	C_{car}–OH	5.62	**c10**	53.06	**TS35**	62.24	**c12**	59.20	NH_2-rot	6.11
b9	22.05	**TS12**	24.37	**b3**	23.45	NH2-rot	1.62	**c9**	50.85	**TS36**	58.71	**c10**	53.06	*H-vibration*	6.76
b4	26.29	**TS13**	28.03	**b6**	27.05	NH2-rot	1.36	**d2**	54.17	**TS37**	56.44	**d1**	55.40	NH_2-rot	1.65
b7	23.68	**TS14**	47.76	**b4**	26.29	C_{car}–C_α	22.78	**e2**	56.47	**TS38**	57.99	**e1**	56.85	NH_2-rot	1.33
b5	20.86	**TS15**	54.02	**b9**	22.05	C_{car}–C_α	32.56	**e1**	56.85	**TS39**	64.64	**e3**	62.68	C_{car}–OH, NH_2-rot	4.87
b9	22.05	**TS16**	29.83	**b4**	26.29	C_{car}–OH	5.66	**a2**	0.00	**TS40**	50.77	**b7**	23.68	*H-shift*	38.93
b5	20.86	**TS17**	28.06	**b7**	23.68	C_{car}–OH	5.79	**a4**	0.95	**TS41**	51.89	**b2**	24.93	*H-shift*	38.95
c1	62.45	**TS18**	65.27	**c3**	62.94	C_α–C_β	2.58	**b6**	27.05	**TS42**	83.97	**c10**	53.06	*H-shift*	43.91
c4	60.33	**TS19**	65.83	**c1**	62.45	C_α–C_β	4.44	**b8**	27.06	**TS43**	84.19	**c12**	59.20	*H-shift*	41.05
c1	62.45	**TS20**	67.14	**c2**	62.47	C_{car}–C_α	4.68	**d2**	54.17	**TS44**	67.12	**c6**	60.48	*cyclization*	9.79
c6	60.48	**TS21**	66.13	**c2**	62.47	C_α–C_β	4.65	**d1**	55.40	**TS45**	63.41	**c14**	58.51	*cyclization*	6.46
c11	59.18	**TS22**	64.93	**c12**	59.20	C_{car}–OH	5.74	**c9**	50.85	**TS46**	67.00	**e3**	62.68	*cyclization*	10.23
c4	60.33	**TS23**	69.68	**c3**	62.94	C_α–C_β	8.05	**c13**	60.69	**TS47**	64.44	**e2**	56.47	*cyclization*	5.86
c8	62.90	**TS24**	66.79	**c3**	62.94	C_{car}–C_α	3.87								

As can be seen from this table, the isomerization of [β-Ala–H]$^-$ underwent 4 hydrogen transfers. In the first two steps, **a2** goes through the transition state **TS40** to **b7**, and **a4** goes through the transition state **TS41** to **b2**, respectively. These two steps are accompanied by the transfer of negative charge from CO_2 to α-C. In the last two steps, **b6** goes through the transition state **TS42** to **c10**, and **b8** goes through the transition state **TS43** to **c12**, respectively. These two steps are accompanied by the transfer of negative charge from α-C to β-C. After that, the isomerization process from species **c** to **d** and **e** is that **c6** goes through the transition state **TS44** to **d2**, **c14** goes through the transition state **TS45** to **d1**, and **c9** goes through the transition state **TS46** to **e3**. In all these three stages of isomerization, a new *σ* bond is formed between the carboxyl group carbon atom and β-C, and a negative charge is transferred from β-C to the oxygen atom bonded only to the chiral carbon atom.

Combined with the data given in the table, it can be found as the following. First, the reaction barrier ($\Delta G^{\neq}$) required for isomerization within each type of ions is mostly maintained within 9 kcal·mol^{-1}. Only 3 steps of isomerization of species **b** ions which is carboxyl rotation have a higher $\Delta G^{\neq}$ (22.5 ~ 32.6 kcal·mol^{-1}). This is because the double bond oxygen atom, the carboxyl carbon atom and the negatively charged α-C form the conjugation structure, so that the bonding between C_{car}–C_{α} is not simple *σ* bond and *π* bond, but between single and double conjugation structure, and the *σ* bond contained in C_{car}–C_{α} requires more energy from the system during rotation. Second, the $\Delta G^{\neq}$ required for isomerization between different species is higher, especially for hydrogen transfer from species **a** to **b** and from **b** to **c** (38.93 ~43.91 kcal·mol^{-1}). It is investigated that the barrier required for isomerization between species **c** and **d** as well as between species **c** and **e** is not high, this is owing to the process from species **c** to **d** or **e** is a loop forming process accompanied by charge transfer from β-C to oxygen atom. Under the interaction of charge transfer and loop forming tension, the barrier required for isomerization is not high.

3.2 H_2O-loss reaction of [β-Ala–H]$^-$

The potential energy profile of H_2O-loss pathways of [β-Ala–H]$^-$ were shown in Figure 2. All the energies given in the figure are relative Gibbs free energies (R.G., kcal·mol^{-1}) obtained with **a2** as reference point.

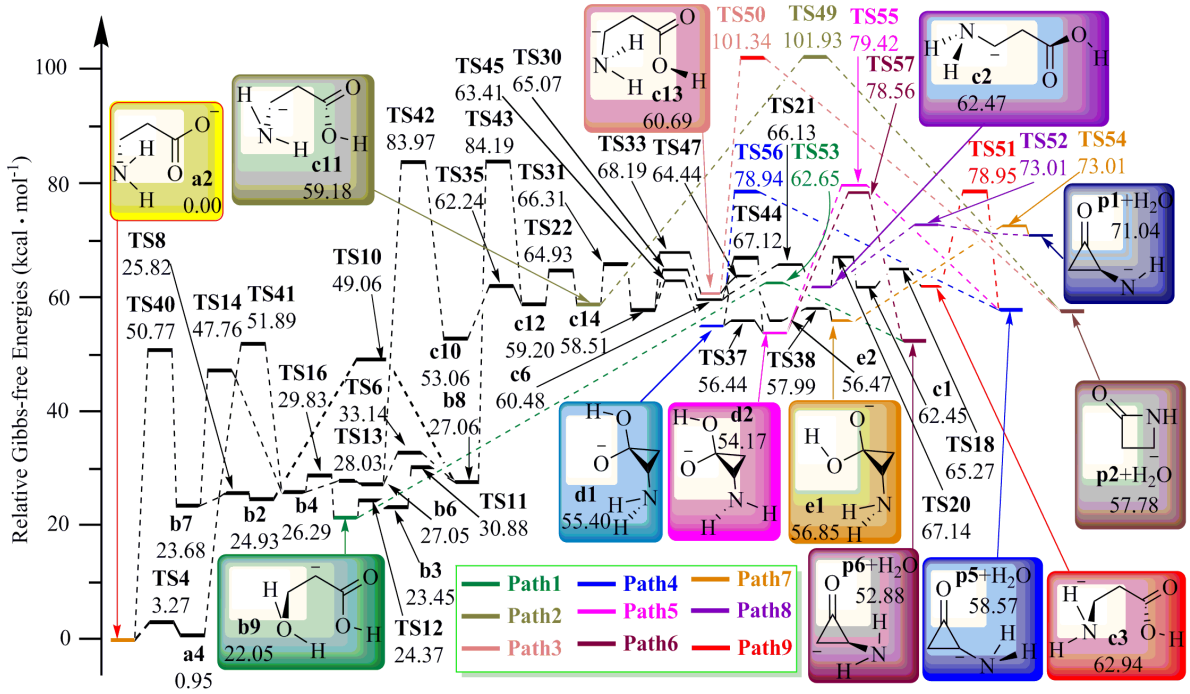

Figure 2: Potential energy profile of H_2O-loss fragmentation reaction computed at the B3LYP/6-311++G(2df,2pd) level of theory with the temperature of 473.15 K

As can be seen from Figure 2, the initial reactant **a2** undergoes a series of isomerization processes to the isomers **b9**, **c2**, **c3**, **c11**, **c13**, **d1**, **d2** and **e1** that can directly undergo pyrolysis reaction. The resulting products after dehydration are **p1**, **p2**, **p5** and **p6**, respectively. **Path 1** and **Path 6** correspond to the same product **p6**, **Path 2** and **Path 3** correspond to the same product **p2**, **Path 4**, **Path 5** and **Path 9** correspond to the same product **p5**, and **Path 7** and **Path 8** correspond to the same product **p1**. The reactant **d2** is dehydrated in two different fragmentation pathways, resulting in two different products **p5** and **p6**, respectively. According to reaction thermodynamics, the reaction Gibbs-free energies ($\Delta_r G$) of **Paths 1 ~ 9**

are all greater than 0 kcal·mol^{-1}, indicating that all the 9 reaction pathways are forward non-spontaneous reactions. Among the four products, **p1** has the highest energy and is the most unstable, **p2** and **p5** have similar energy, and **p6** has the lowest energy and is the most dominant product. According to reaction kinetics, the reaction barriers of **Path 2** and **Path 3** were the two highest among the nine reaction pathways, and the rate-determine steps of **Paths 4 ~ 9** were all determined by **TS42**. **Path 1** had a relatively low reaction barrier ($\Delta G^{\neq}_{TS53}$ = 62.65 kcal·mol^{-1}), which was more advantageous than other H_2O-loss pathways. Therefore, **Path 1** was the dominant pathway in the H_2O-loss reaction of [β-Ala–H]$^-$ ions, and the corresponding product **p6** was also the dominant product in all the dehydration products.

3.3 NH_3-loss reaction of [β-Ala–H]$^-$

The potential energy profile of NH_3-loss pathways of [β-Ala–H]$^-$ were shown in Figure 3. All the energies given in the figure are relative Gibbs free energies (R.G., kcal·mol^{-1}) obtained with **a2** as reference point.

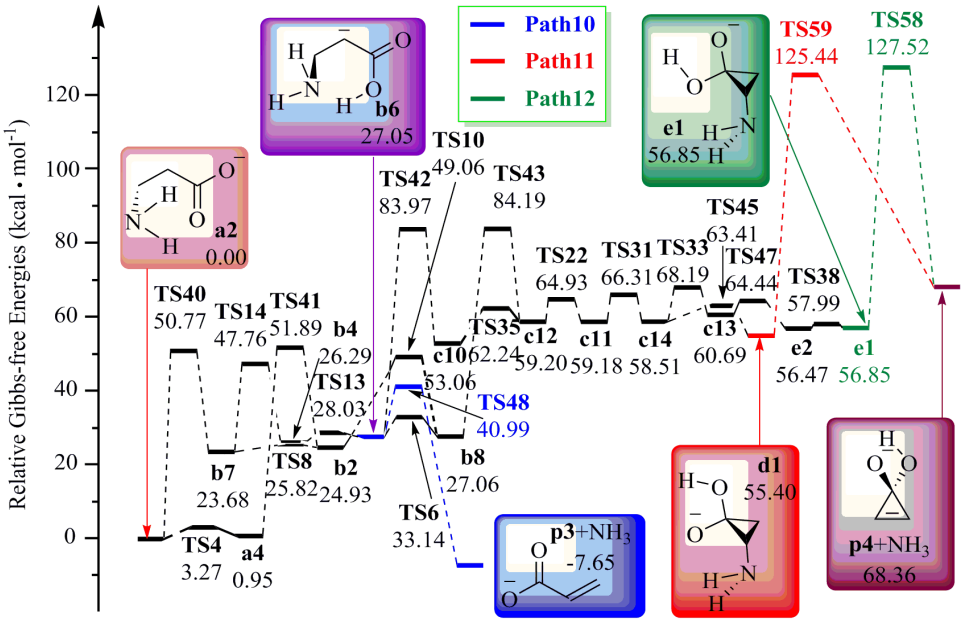

Figure 3: Potential energy profile of NH_3-loss fragmentation reaction computed at the B3LYP/6-311++G(2df,2pd) level of theory with the temperature of 473.15 K

It can be seen from the three response pathways that the decisive steps of **Paths 10 ~ 13** are **TS48**, **TS59** and **TS58** respectively. According to the reaction thermodynamics, only reaction Gibbs-free energy ($\Delta_r G$) of **Path 10** is less than 0 kcal·mol^{-1} among the three reaction pathways, the other reactions are all positive non-spontaneous reactions, and the product **p3** is also the dominant product among all the deamination products. According to the reaction kinetics, **Paths 11 ~ 12** have the highest reaction barriers ($\Delta G^{\neq}$) which value are above 125 kcal·mol^{-1}. However, the potential barrier of the rate-determine step (**TS40**) of **Path 10** is only 50.77 kcal·mol^{-1}. Therefore, **Path 10** is the most dominant pathway among the three NH_3-loss pathways of [β-Ala–H]$^-$.

3.4 Temperature dependence of the H_2O- and NH_3-loss reaction

In order to investigate the influence of temperature on the reaction pathways and products, the reference point **a2**, the transition states of the rate-determining steps in the reaction pathways and transition states that are close to the energy of the rate-determining steps, the products after dehydration and deamination, and two neutral molecules, NH_3 and H_2O, were selected for frequency analysis and calculated the thermodynamic data. The selected temperature range is 273.15 ~ 853.15K, and the interval temperature is 20 K. The results are shown in Figure 4.

As can be seen from Figure 4, the influence of temperature on dehydration and deamination of [β-Ala–H]$^-$ ions is basically controlled within 4 kcal·mol^{-1}. Figure 4 shows the curves of energy variation with temperature of all possible rate-determination steps (the transition state in which the difference of Gibbs-free energy is less than 2 kcal·mol^{-1}) of H_2O- and NH_3-loss pathways. Figure 4(a) shows the curves of rate-determination steps of H_2O-loss pathways with temperature change, and Figure 4(b) shows the curves of rate-determination steps of NH_3-loss pathways with temperature change.

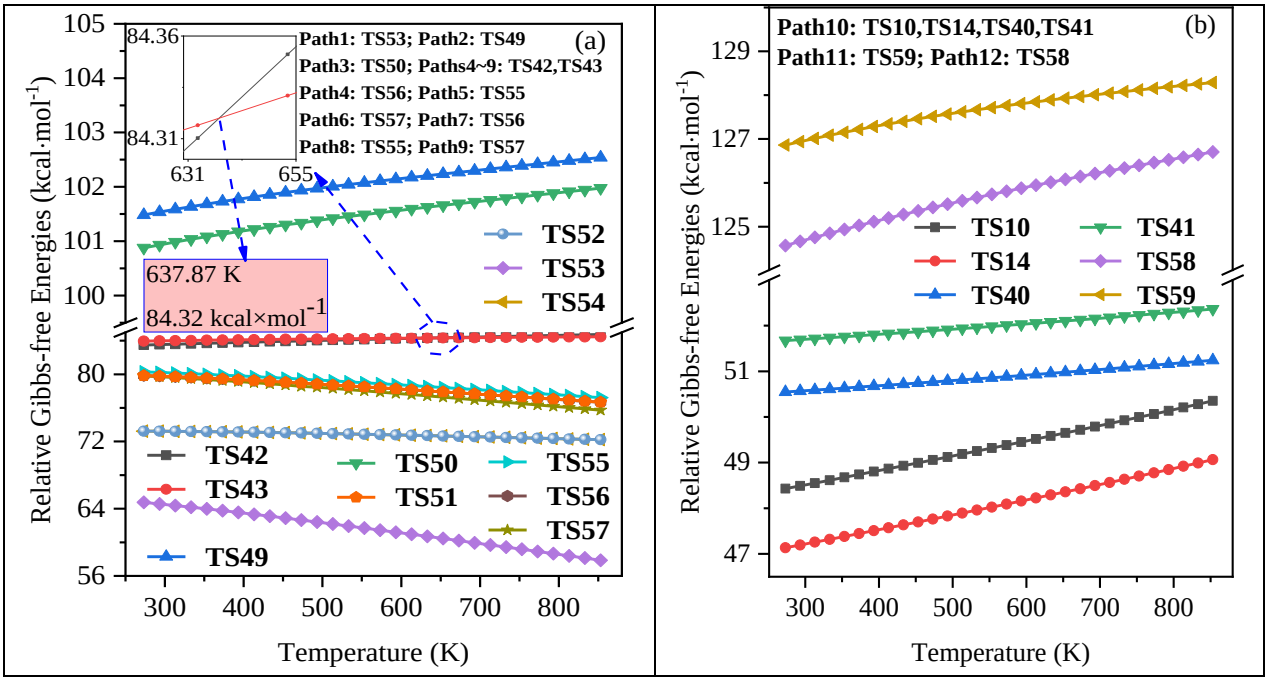

Figure 4: Temperature dependence of the rate-determining steps for the H_2O- (a) and NH_3-loss (b) reactions computed at the B3LYP/6-311++G(2df,2pd) level of theory.

As shown in Figure 4(a), the rate-determining steps of H_2O-loss pathways **Paths 4 ~ 9** is **TS42** and **TS43**, whose energy is changed less than 1 kcal·mol^{-1} with the temperature increasing. Among them, **TS42** increases slowly with the increase of temperature, while **TS43** is the opposite. The energy of **TS42** and **TS43** is equal at 637.87K ($\Delta G^{\neq}$ = 84.32 kcal·mol^{-1}). The rate-determining step of **Path 1** is **TS53**, whose energy changes with temperature increasing is 6.89 kcal·mol^{-1}, which is the largest energy change among the 6 H_2O-loss reaction pathways and the only rate-determining step whose energy changes exceed 5kcal·mol^{-1} among all reaction pathways. What is unique is that the reaction barrier of the rate-determining step of **Path 1** is the one with the lowest energy in all the dehydration reactions, and the barrier decreases obviously with the increasing temperature. Therefore, **Path 1** was always the optimal path in H_2O-loss reaction when the temperature was controlled at 273.15 ~ 853.15 K.

Figure 4(b) shows the curve of the rate-determining step of the NH_3-loss pathways changing with temperature. Among them, **TS58** and **TS59** were the decisive steps of **Path 12** and **Path 11** respectively, and **TS10**, **TS14**, **TS40** and **TS41** were the possible decisive steps of **Path 10**. The energy variation of all the determined or possible deamination steps is within 2 kcal·mol^{-1}, and all of them increased with the temperature increasing. As can be seen from this figure, **Paths 11 ~ 12** are the two reaction paths with the highest energy among the three deamination reaction paths. Combined with the deamination reaction analysis in Figure 3, the deamination reaction of **Path 10** with **TS48** as the deamination symbol can be divided into two paths starting from **a2** to **b6** that can directly deaminate. The possible speed limiting steps of the first branch path are **TS10** and **TS41**, and the possible speed limiting steps of the second branch path are **TS14** and **TS40**. Obviously, **TS40** is a relatively low speed determination step in the two paths. Therefore, in combination with Figure 3 and Figure 4(b), it is not difficult to conclude that in the temperature range of 273.15 ~ 853.15K, the optimal choice of **Path 10** is from **a2** to **b6** through **TS40**, and then directly deaminate product **p3** through **TS48**. In addition, **Path 10** is always the optimal path in the deamination reaction.

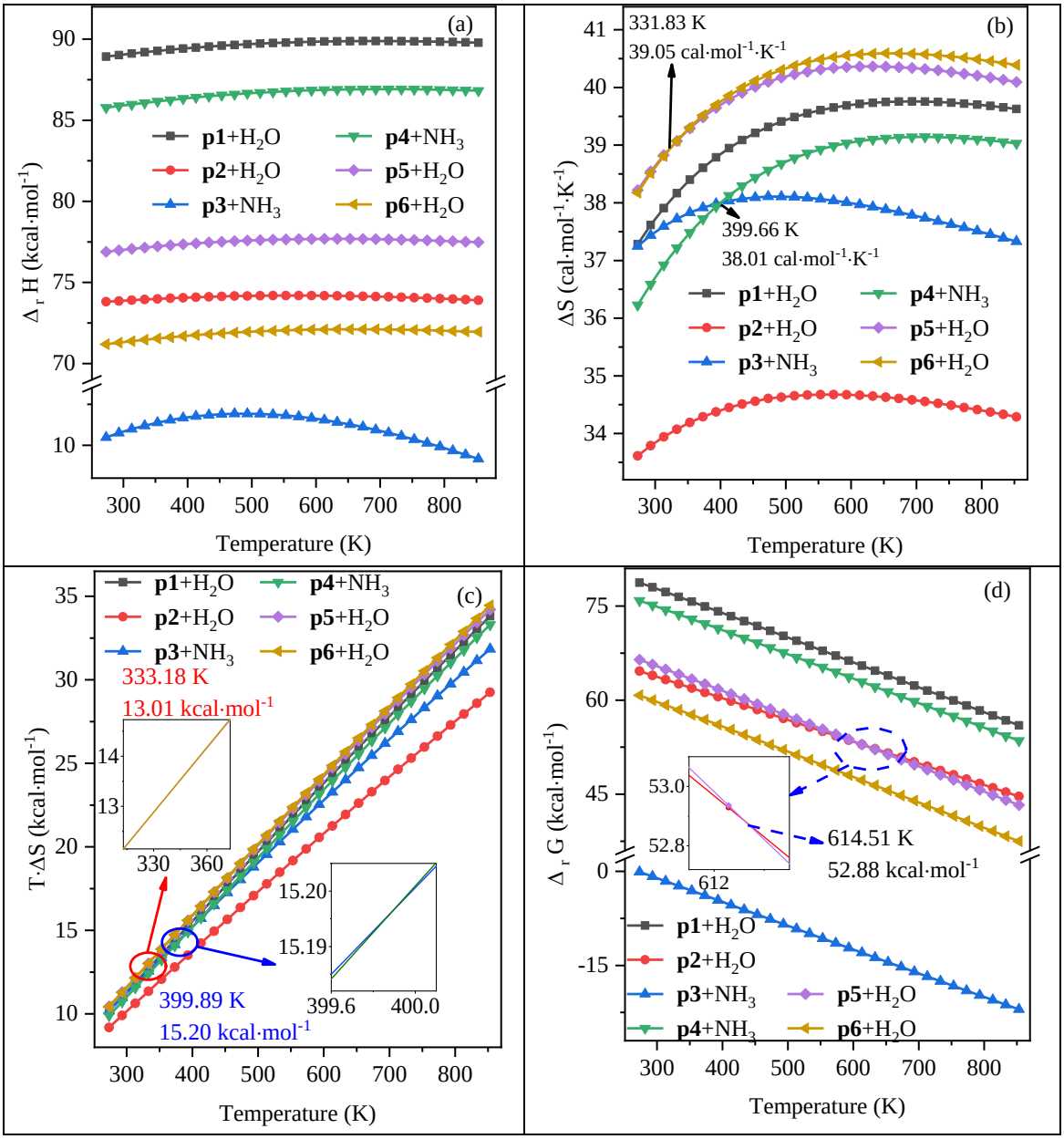

Figure 5: Temperature dependence of the reaction enthalpies ($\Delta_r H$) (a), reaction entropies (($\Delta_r S$)) (b), $T\cdot\Delta_r S$ (c), and reaction Gibbs free energies ($\Delta_r G$) (d) for the fragmentation reactions starting from reactant a2 computed at the B3LYP/6-311++G(2df,2pd) level of theory

Figure 5 shows the thermodynamic data variation curves of four H_2O-loss products and four NH_3-loss products with the increasing temperature. It can be seen from Figure 5(a) that the reaction enthalpies ($\Delta_r H$) of the NH_3-loss products is lower than that of the H_2O-loss products, while **p3** is the most dominant product among all the H_2O-loss and NH_3-loss products, and the $\Delta_r H$ of all products changes very little with the increasing temperature. As shown in Figure 5(b), the reaction entropy ($\Delta_r S$) of different reactants shows energy staggered with the temperature increasing, but all the entropy increases greatly with the temperature increase at the beginning, and decreases slowly with the temperature change after reaching a critical point. All $\Delta_r S$ vary within 4 cal·mol^{-1}·K^{-1} in the temperature range of 273.15 ~ 853.15 K. Figure 5(c) shows a significant linear increase in $T\cdot\Delta_r S$ for different reactants, which is affected by temperature rather than $\Delta_r S$. The deamination products **p3** and **p4** showed $T\cdot\Delta_r S$ interleaving at 399.86 K, and the deamination products **p5** and **p6** showed $T\cdot\Delta_r S$ interleaving at 333.18 K. It can be seen from Figure 5(d) that $\Delta_r G$ of all reactants decreases linearly with the increase of temperature. The energies of deamination products are higher than that of deamination products. When the temperature is lower than 614.51 K, deamination product **p2** is more dominant than **p5**, and when the temperature is higher than this, **p5** is more dominant than **p2**, but deamination product **p3** is still the most dominant product in thermodynamics. Based on Figure 5, it is not difficult to see that the deamination product **p3** is the most

advantageous product of [β-Ala–H]$^-$ ion fragmentation mechanism in thermodynamics.

4. CONCLUSION

The reaction mechanism of [β-Ala–H]$^-$ at B3LYP/6-311++G(2df,2pd) level with the temperature of 473.15 K shows that H_2O- and NH_3-loss reaction could be realized when the energy provided by the environment was higher than 62.65 kcal·mol^{-1}. The details are listed below.

1. In the process of isomerization of [β-Ala–H]$^-$, the reaction barriers ($\Delta G^{\neq}$) required for hydrogen transfer is the highest; and the carboxyl rotation of **b** is affected by conjugation, whose $\Delta G^{\neq}$ is higher than that of other σ bond rotations. The $\Delta G^{\neq}$ is basically within 10 kcal·mol^{-1} for σ bond rotation internal and isomerize among **c**, **d** and **e**.
2. The dominant H_2O-loss pathway of [β-Ala–H]$^-$ is **Path 1**, and the corresponding product **p6** is also the dominant product. The dominant NH_3-loss pathway of [β-Ala–H]$^-$ is **Path 10**, and the corresponding product **p3** is also the dominant product. From the perspective of thermodynamics, the reaction pathway **Path 10** corresponding to NH_3-loss product **p3** is the unique reaction pathway that can proceed spontaneously in the forward direction, and **p3** is also the most dominant product in all the H_2O- and NH_3-loss pathways. However, from the perspective of reaction kinetics, the $\Delta G^{\neq}$ of NH_3-loss pathway **Path 10** is also the lowest, which is the most dominant reaction pathway among all the reaction pathways.
3. It is investigated that only the rate-determine step of **Paths4 ~ 9** changed with the temperature increasing (273.15 K ~ 573.15 K), while the dominant pathway of all H_2O- and NH_3-loss reaction did not change, and the corresponding dominant products did not change either.

Fund project: "Three Longitudinal" Youth Innovative Talent Project of Heilongjiang Bayi Agricultural University (ZRCQC202010); Daqing City guiding science and technology project (zd-2021-88); Doctoral Research Foundation of Heilongjiang Bayi Agricultural University (XDB202112).

Author's brief introduction: Quan Sun (1990-), man, Master's Degree, Assistant laboratory Technician, Corresponding author, mainly engaged in theoretical study on the reaction mechanism of substances.

REFERENCE

1. Kasschau, M. R., Skisak, C. M., Cook, J. P., & Mills, W. R. (1984). β-Alanine metabolism and high salinity stress in the sea anemone, Bunodosoma cavernata. *Journal of Comparative Physiology B*, *154*(2), 181-186.
2. Hoffman, J. R., Emerson, N. S., & Stout, J. R. (2012). β-alanine supplementation. *Current Sports Medicine Reports*, *11*(4), 189-195.
3. Stellingwerff, T., Decombaz, J., Harris, R. C., & Boesch, C. (2012). Optimizing human in vivo dosing and delivery of β-alanine supplements for muscle carnosine synthesis. *Amino acids*, *43*(1), 57-65.
4. Toggenburger, G., Felix, D., Cuénod, M., & Henke, H. (1982). In vitro release of endogenous β-alanine, GABA, and glutamate, and electrophysiological effect of β-alanine in pigeon optic tectum. *Journal of Neurochemistry*, *39*(1), 176-183.
5. Choquet, D., & Korn, H. (1988). Does β-alanine activate more than one chloride channel associated receptor?. *Neuroscience letters*, *84*(3), 329-334.
6. Sandberg, M., & Jacobson, I. (1981). β-Alanine, a possible neurotransmitter in the visual system?. *Journal of Neurochemistry*, *37*(5), 1353-1356.
7. Buc, S. R., Ford, J. H., & Wise, E. C. (1945). An improved synthesis of β-alanine. *Journal of the American Chemical Society*, *67*(1), 92-94.
8. Miao, Y., Liu, J., Wang, X., Liu, B., Liu, W., & Tao, Y. (2022). Fatty acid feedstocks enable a highly efficient glyoxylate-TCA cycle for high-yield production of β-alanine. *mLife*, 1(2), 171-182.
9. Hobson, R. M., Saunders, B., Ball, G., Harris, R. C., & Sale, C. (2012). Effects of β-alanine supplementation on exercise performance: a meta-analysis. *Amino acids*, *43*(1), 25-37.
10. Hoffman, J., Ratamess, N. A., Ross, R., Kang, J., Magrelli, J., Neese, K., ... & Wise, J. A. (2008). β-Alanine and the hormonal response to exercise. *International journal of sports medicine*, *29*(12), 952-958.
11. Bellinger, P. M. (2014). β-Alanine supplementation for athletic performance: an update. *The Journal of Strength & Conditioning Research*, *28*(6), 1751-1770.
12. Juaristi, E., Ed. (1997). Enantioselecti Ve Synthesis of -Amino Acids; *Wiley*: New York.
13. Juaristi, E., & Soloshonok, V. (2005). Enantioselecti Ve Synthesis of -Amino Acids, 2nd ed.; *Wiley*: New York.
14. Tiedje, K. E., Stevens, K., Barnes, S., & Weaver, D. F. (2010). β-Alanine as a small molecule neurotransmitter. *Neurochemistry international*, *57*(3), 177-188.
15. Décombaz, J., Beaumont, M., Vuichoud, J., Bouisset, F., & Stellingwerff, T. (2012). Effect of slow-release β-alanine tablets on absorption kinetics and paresthesia. *Amino acids*, *43*(1), 67-76.
16. Tan, C. Y. K., Wainman, D., & Weaver, D. F. (2003). N-, α-, and β-substituted 3-aminopropionic acids: design, syntheses and antiseizure activities. *Bioorganic & medicinal chemistry*, *11*(1), 113-121.
17. Meenukutty, M. S., Mohan, A. P., Vidya, V. G., & Kumar, V. V. (2022). Synthesis, characterization, DFT analysis and docking studies OFA novel schiff base using 5-bromo salicylaldehyde and β-

alanine. *Heliyon*, e09600.

18. Delkov, D., Yoanidu, L., Tomov, D., Stoyanova, R., Dechev, I., & Uzunova, Y. (2022). Oncometabolites in urine-a new opportunity for detection and prognosis of the clinical progress of verified prostate cancer-a pilot study. *Turkish Journal of Medical Sciences*, *52*(3), 699-706.
19. Ehrenfreund, P., Glavin, D. P., Botta, O., Cooper, G., & Bada, J. L. (2001). Extraterrestrial amino acids in Orgueil and Ivuna: Tracing the parent body of CI type carbonaceous chondrites. *Proceedings of the National Academy of Sciences*, *98*(5), 2138-2141.
20. Blagojevic, V., Petrie, S., & Bohme, D. K. (2003). Gas-phase syntheses for interstellar carboxylic and amino acids. *Monthly Notices of the Royal Astronomical Society*, *339*(1), L7-L11.
21. Papavinasam, E., Natarajan, S., & Shivaprakash, N. C. (1986). Reinvestigation of the crystal structure of β-alanine [J]. *International Journal of Peptide and Protein Research*, 28(5), 525-528.
22. Jose, P., & Pant, L. M. (1965). The crystal and molecular structure of β-alanine. *Acta Crystallographica*, *18*(4), 806-810.
23. Jose, P., & Pant, L. M. (1965). The crystal and molecular structure of β-alanine. *Acta Crystallographica*, *18*(4), 806-810.
24. Papavinasam, E., Natarajan, S., & Shivaprakash, N. C. (1986). Reinvestigation of the crystal structure of β-alanine. *International Journal of Peptide and Protein Research*, *28*(5), 525-528.
25. Abraham, R. J., & Hudson, B. D. J. (1976). Rotational isomerism—XXI11 Pt XX, Abraham, R. J., & Loftus, P. J. Chem. Soc. Perkin Trans. II, 1142: The conformation of 2-amino-3-fluoropropanoic acid (2-afp) and 2-fluoro-3-aminopropanoic acid (3-afp) as the zwitterion, cation and anion, an nmr a [J]. *Journal of the Chemical Society*, Perkin Transactions. I1 1986, 1635-1640.
26. McGlone, S. J., & Godfrey, P. D. (1995). Rotational Spectrum of a Neurohormone:. beta.-Alanine. *Journal of the American Chemical Society*, *117*(3), 1043-1048.
27. Sanz, M. E., Lesarri, A., Peña, M. I., Vaquero, V., Cortijo, V., López, J. C., & Alonso, J. L. (2006). The shape of β-alanine. *Journal of the American Chemical Society*, *128*(11), 3812-3817.
28. Eckersley, M., Bowie, J. H., & Hayes, R. N. (1989). Collision-induced dissociations of deprotonated α-amino acids. The occurrence of specific proton transfers preceding fragmentation. *International journal of mass spectrometry and ion processes*, *93*(2), 199-213.
29. Choi, S. S., & Kim, O. B. (2013). Fragmentation of deprotonated amino acids in atmospheric pressure chemical ionization. *International Journal of Mass Spectrometry*, *338*, 17-22.
30. Sun, Q., & Yu, H. T. (2018). A density functional theory investigation of the fragmentation mechanism of deprotonated asparagine. *Computational and Theoretical Chemistry*, *1141*, 45-52.
31. Bak, K. L., Jo/rgensen, P., Helgaker, T., Ruud, K., & Jensen, H. J. R. A. (1993). Gauge-origin independent multiconfigurational self-consistent-field theory for vibrational circular dichroism. *The Journal of chemical physics*, *98*(11), 8873-8887.
32. Lee, C., Yang, W., & Parr, R. G. (1988). Development of the Colle-Salvetti correlation-energy formula into a functional of the electron density. *Physical review B*, *37*(2), 785-789.
33. Miehlich, B., Savin, A., Stoll, H., & Preuss, H. (1989). Results obtained with the correlation energy density functionals of Becke and Lee, Yang and Parr. *Chemical Physics Letters*, *157*(3), 200-206.
34. Frisch, M. J., Pople, J. A., & Binkley, J. S. (1984). Self-consistent molecular orbital methods 25. Supplementary functions for Gaussian basis sets. *The Journal of chemical physics*, *80*(7), 3265-3269.
35. Frisch, M. J., Trucks, G. W., Schlegel, H. B., Scuseria, G. E., Robb, M. A., Cheeseman, J. R., ... & Fox, D. J. (2009). Gaussian 09, Revision D. 01, Gaussian, Inc., Wallingford CT. *See also: URL: http://www. gaussian. com*.